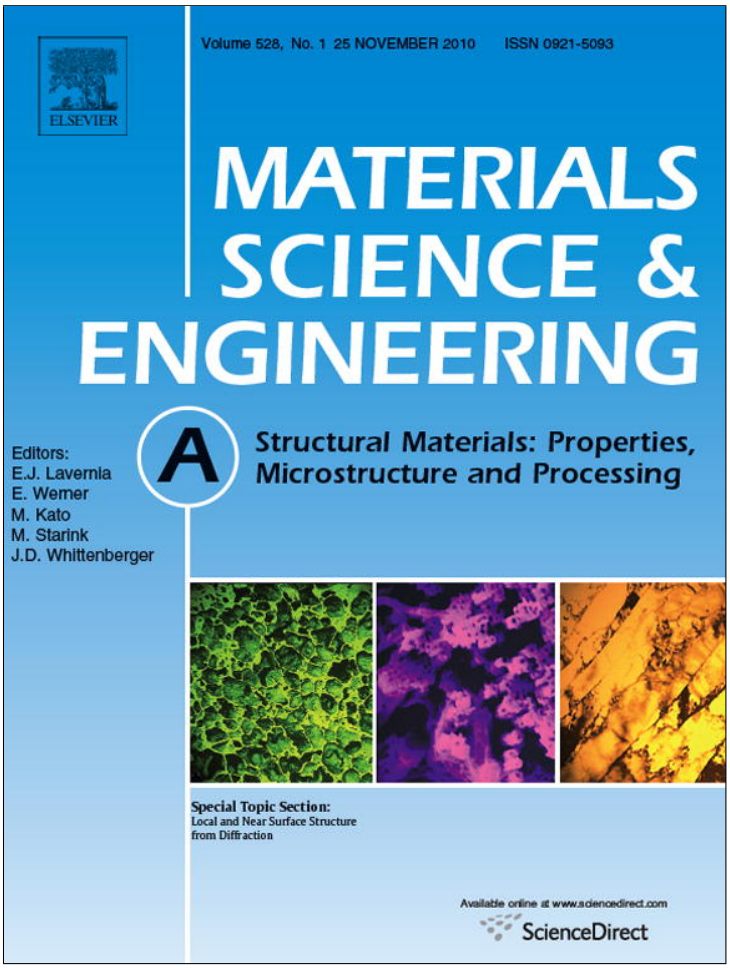

Materials Science and Engineering A 528 (2010) 37–51

Contents lists available at ScienceDirect

Materials Science and Engineering A

journal homepage: www.elsevier.com/locate/msea

Voyaging around nacre with the X-ray shuttle: From bio-mineralisation to prosthetics via mollusc phylogeny

D. Chateigner[a,*], S. Ouhenia[a,b], C. Krauss[a], C. Hedegaard[a,1], O. Gil[c], M. Morales[d], L. Lutterotti[e], M. Rousseau[f], E. Lopez[g]

[a] CRISMAT-ENSICAEN, IUT-Caen, Université de Caen Basse-Normandie, 6 Bd. M. Juin, 14050 Caen, France
[b] Lab. De Physique, Faculté des Sciences Exactes, Bejaia 06000, Algeria
[c] ERPCB, IUT-Caen, Université de Caen Basse-Normandie, 6 Bd. M. Juin, 14050 Caen, France
[d] CIMAP-ENSICAEN, Université de Caen Basse-Normandie, 6 Bd. M. Juin, 14050 Caen, France
[e] Department of Materials Engineering, Engineering Faculty, University of Trento, via Mesiano, 77 – 38123 Trento, Italy
[f] UMR 7561 CNRS, Nancy University, BP184, 54505 Vandoeuvre les Nancy,France
[g] UMR7208 BOREA, CNRS/Muséum National d'Histoire Naturelle, 43, rue Cuvier 75231, Paris Cedex 05, France

ARTICLE INFO

Article history:
Received 7 April 2010
Received in revised form 8 July 2010
Accepted 12 July 2010

Keywords:
Mollusc
Phylogeny
Nacre
Biomimetics
Aragonite
Calcite
Fossils

ABSTRACT

Strong textures of mollusc shell layers are utilised to provide phylogenetic information. Aragonitic and calcitic layers are the targets here, inside which nacre layers, but not only, play a specific role. At the light of the texture patterns and a parcimonious approach, nacre appears not as an ancestral form of calcium carbonate in mollusc layers. Also, from texture terms we can propose some links to ancestral fossilised species. The aragonite unit-cell distortions due to macromolecule complex insertions in the microstructures are measured on raw specimens for several aragonite layers of gastropods and bivalves. The textural information is used to provide precise structural determination of the biogenic aragonite. Such information might provide useful lights on the biomineralisation processes in the future, in cladistic approaches. Farming conditions are shown not to influence much shell textures of *Helix aspersa aspersa*. Closely related species exhibit globally close textures, among which three are good candidates for bone neogeneration and which textures are identical. Electrodeposition of aragonite, with inclusion of molecular extract from shell species, results in nacre-like layers exhibiting structural distortions similar to known inductive layers. X-ray diffraction experiments are shown to provide invaluable insights in testing biomineralisation and phylogenetic hypotheses.

1. Introduction

The fascinating organic-mineral biocomposites constituting mollusc shells consist in nanometre-size growth-control of calcium carbonate crystals with only 1–5 wt.% of organic material [1,2]. This achieves considerable increase of the shell toughness compared to the non-biogenic mineral and high mechanical performances. Nacre hardness from the red abalone *Haliotis rufescens*, is 3000 times larger than the one of the mineral [3–5], attributed to strong structural bounds between organic macromolecules and inorganic crystals [6,7]. Mollusc shells are to a large phylogenetic extent, mainly made of calcite and aragonite crystalline polymorphs. The major part of organic materials is intercrystalline, and in a minor way intracrystalline, both dedicated to specific, and somehow still undetermined, roles. Recently, Pokroy et al. [8,9] demonstrated the anisotropic deformations of the biogenic unit-cells attributed to intracrystalline organic molecules. This corresponds to a stabilisation of the metastable biogenic aragonite via intermediate aplanarity of the carbonate groups, between a perfect plane for calcite and non-biogenic aragonite [10].

Bobbio [11] analysed Maya cranes exhibiting nacre teeth with an ante-mortem character, showing bone growth around nacre, hereby demonstrating the oldest signature of human implantology, and using natural mollusc shells. The possibility of natural and biogenic exoskeleton osteointegration in human bones was born, opening the way to dentistry and prosthetics in general. It needed about two decades to promote this idea further, with the demonstrations that natural nacre from the mother of pearl oyster *Pinctada maxima* is not only biocompatible but osteoinductive for rabbit and sheep bones [12], and even stimulate bone generation by human osteoblasts in vitro [13] and in vivo [14]. These fascinating

* Corresponding author. Tel.: +33 02314 52611; fax: +33 02319 51600.
E-mail address: daniel.chateigner@ensicaen.fr (D. Chateigner).

[1] This paper is dedicated to Claus Hedegaard, deceased at the age of 46. Mineralogist, palaeontologist, malacologist, Claus will remain in our minds as a rare and vivid friend, initiating and making science.

0921-5093/$ – see front matter © 2010 Elsevier B.V. All rights reserved.
doi:10.1016/j.msea.2010.07.032

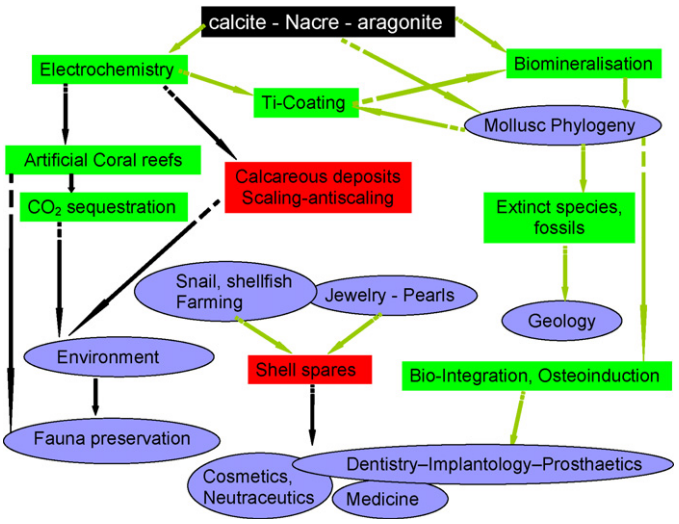

Fig. 1. Schematic representation of calcium carbonate implications (green arrows) and potential implications (dark arrows). (For interpretation of the references to color in this figure legend, the reader is referred to the web version of the article.)

discoveries gave rise to a huge number of research developments at the interfaces of several scientific disciplines (Fig. 1). Important works demonstrated nacre powder stimulation effect of cutaneous fibroblasts of rats [15], and lipids extracted from the nacre of *Pinctada margaritifera* showed restoration signals on artificially dehydrated skin explants [16]. The potentials of nacre in dermatology and cosmetics combined to its prosthetic utilities would allow large use of actual spares resulting from shellfish farmings (oysters, snails, pearl industry, etc.). Aragonitic deposits are also present as scales in industry, where they penalise energy transfers, fluid exchange. Such scaling is the result either of precipitation of calcium carbonate under various working conditions, among which temperature and pH appear as major parameters, or of electrochemical processes. Antiscaling can also be driven using electrochemistry, and may be used for the formation of large structures like artificial coral reefs, with a non-negligible and positive impact on fauna and environment, notably through CO_2 sequestration. We recently used electrodeposition to synthesise calcium carbonate layers on Ti–6Al–4V substrates, in the aim of mimicking nacre microstructures [17]. Such purely inorganic nacre-like layers are the first step toward organic–inorganic composites to coat Ti-based prostheses with a priori no shape limitation. On one hand, biomineralisation understanding would be an invaluable guide in the optimisation of such coatings. On the other hand, their full characterisation might give light on biomineralisation processes, and on the complex architecture of nacre (or any osteogenic form of calcium carbonate), which has been the target of so many works [18–25]. One way to observe biomineralisation effect is to look at mollusc phylogeny. Dealing with mollusc shell, one can approach some differences using for instance X-ray diffraction. In particular, crystallographic texture analysis was proved to deserve character analysis on many different taxa [26,27], and even helped to link some fossil ancestor [28]. Of particular interest is the fact that species showing interesting behaviours in terms of medical applications (*P. maxima* [14], *P. margaritifera* [29], *Pinna nobilis*, *Haliotis tuberculata*), also exhibit peculiar texture terms, these latter acquiring then a potentially predictive character. The existence of this strong intrication between biomineralisation, texture patterns and osteogenic properties, motivated an abundant literature around calcium carbonate and nacre.

In this paper we enlarge our mollusc phylogeny sampling, including several bivalves, gastropods, cephalopods and fossils, and calcitic layers. We extend the analysis not only to texture patterns, but also to structure modifications (unit-cell distortions and motif), at the light of the pionneering works of Pokroy et al. [8–10]. Concerning mollusc nacres we use the texture terms to propose an idea of classification, which allows a smaller number of events in the phylogeny than in the commonly accepted views. Calcitic layers of some fossils are measured and compared to calcite layers of extant species. We then show that using electrodeposition, organic–inorganic composite layers can be deposited on titanium substrates, which show structural distortions close to the ones encountered in some natural species. A detour is made to show that usual snail farming and selection conditions do not influence much shell crystallisation, and that X-ray investigations are operated within reasonably good repeatability on natural shell samples.

2. Materials

Many resources provided shell specimens. The University of California Museum of Paleontology (UCMP), at Berkeley-USA, the United State National Museum of Natural History (USNM), the Zoologisk Museum in Copenhagen-Denmark (ZM), the Laboratoire de Biologie et Génétique Evolutive (LBGE), at Le Mans-France, the Department of Earth Sciences collection and our own collections.

The studied specimens range in the bivalves, gastropods, cephalopods and Monoplacophoras. The taxon sampling is skewed towards aragonitic layers, but several calcitic layers are also studied, and we included few fossil species. A detailed description of the microstructural arrangements (nacre, crossed lamellar, etc.) can be found in Hedegaard [30], and we use the usual terminology [31–34] for the denomination of layers. We added to our phylogenic sampling of Chateigner et al. [27], shells and layers from latter works, *Charonia lampas lampas* [35], *Trichite* sp., *P. nobilis*, *Amussium parpiraceum*, *Crassostrea gigas*, *Mytilus edulis*, *Mytilus californianus*, *Bathymodiolus thermophylus*, *Pteria penguin* [28], *Baculitis* sp., *H. tuberculata tuberculata*, *Pilina unguis*, *Mercenaria mercenaria*, *Nautilus macromphalus*, *Cellana testudinaria*, *Neopilina galatheae*, *Acmaea mitra*, *Acila castrensis*, *Anodonta cygnea*, *Tapes japonica*, *Arctica islandica*, *Scutus antipodes*, *Tectus niloticus*, *Phasianela australis*, *Perotrochus quoyanus*, *Scutellastra cochlear*, *Helminthoglypta nickliniana anachoreta*, *Entemnotrochus adansonianus*, *Cypraea mus*, *Cyclophorus woodianus*, *Belemnite* sp.

In order to examine the effect of farming on the shell growth, and to test X-ray measurements repeatability on shells in a difficult case, we investigated two series of *H. aspersa aspersa*. These specimens were issued from a selected for increased weight (S) (14 samples) and a control (C) (15 samples) line [36]. The selection procedure is described in Dupont-Nivet et al. [37], and animals are all reared in the same room with environmental conditions optimal for growth (density, food, temperature, relative humidity, photoperiod).

Electrodeposition was used to elaborate aragonite films on medical-grade titanium foils. We then used several organic additions in the electrolyte in order to test the feasibility of their incorporation in the aragonite structure. We used chitosan, water-soluble and ethanol-soluble extract from the shells of *P. maxima*, using a methodology described elsewhere [38], and optimised electrodeposition conditions [39].

3. Experiments

For all the X-ray experiments we adopted the same main shell direction convention as in previous studies [27], i.e. the growth direction, **G**, perpendicular to the margin of the shell at the beam location is the vertical axis of our pole figures. The plane tangent to the shell at the beam location, defined by the sample holder

plane, has its normal, **N**, as the normal axis of the pole figures. The third axis, **M**, direction of the growth lines is then horizontal on the pole figures. For the neutron study of the *Belemnite* sp., we were however positioning the sample differently for technical reasons, with the revolution axis of the rostrum being the centre of the pole figures. All discussions concerning cell parameter and atomic position distortions refer to the orthorhombic mineral aragonite (COD references no. 2100187 [40], with a purely mineral cell [Pmcn: $a = 4.96183(1)$ Å, $b = 7.96914(2)$ Å, $c = 5.74285(2)$ Å; {x, y, z positions: Ca (0.25, 0.41502(2), 0.75985(4)), C (0.25, 0.76190(1), −0.0823(1)), O1 (0.25, 0.92238(8), −0.09453(8)), O2 (0.47499(7), 0.68013(5), −0.08725(7))}]) as determined by Caspi et al. [41].

All textural and structural analyses added to this work from previous studies were conducted within the combined analysis frame [42], a more complete analysis that allows simultaneous determination of texture and structure with less bias than classical and individual determination of both. This approach was chosen because it allows working on real samples, without grinding operation nor specific preparation. The specimens were polished as flat as possible, and each layer measured successively, from the outer to the inner, by removing capping layers using HCl, inward. After removal we controlled using optical microscopy that no gross remaining part of the layer was present on top of the next to be studied, and using SEM that the expected microstructure was kept. Any eventual phase transformation due to HCl effect has never been detected in X-ray diagrams, and surface roughness introduced during HCl etching was always below 2 μm, not influencing X-ray analysis. For all these experiments, the main directions of the shells were first defined using an optical microscope. Wishing to explore the extent of the phylogenetic signal in textures, we found it practical to use a compact notation based on the actual observations and a systematic nomenclature which helps to compare the species [26].

SEM experiments of fractured shells were carried out either on an electroscan environmental scanning electron microscope (ESEM) at University of California, Museum of Paleontology, or on a Zeiss at CRISMAT Laboratory, both microscopes requiring specimens to be metal coated.

For X-ray diffraction studies, we used 3 different 4-circles diffractometers, all at monochromatic wavelengths. The first instrument (Dept. of Earth Sciences, University of California at Berkeley, USA) uses a point detector and the Fe Kα wavelength, with wide detecting slits [26]. The second and third instruments use the INEL-CPS120 curved position sensitive detector, Cu Kα wavelength and narrow collimation. They offer to treat the data using the full diffraction diagrams, and are held respectively by the Université du Maine, Le Mans France [43], and CRISMAT Laboratory, ENSICAEN France [44]. All instruments give reliable data [45–47]. With point detector, defocusing corrections were operated using standard samples [48] and symmetric geometry, while with curved position sensitive detectors, asymmetric geometry and full pattern analysis, defocusing corrections are not necessary. In this case absorption, volume and localisation corrections were carried out using usual procedures [42]. Classical QTA was done using the Berkeley Texture Package [49], while combined analysis was operated using the MAUD software [50]. We calibrated the X-ray instruments using the LaB_6 standard from NIST.

Neutron experiments were carried out on the D1B beamline, making use of the Eulerian cradle and the CPS detector spanning 80° in 2θ. The "calcite standard" was used previously to calibrate this instrument [51].

For all diffraction experiments we scanned a 5° × 5° regular grid in tilt χ (from 0 to 60° for X-rays and up to 90° with neutrons) and azimuth φ (from 0 to 355°). For *P. maxima* combined analysis measurements we increased the grid resolution to 2.5° for the two angles, resulting in 3744 measured diagrams.

4. Quantitative results of texture analysis

Quantitative texture analysis is used to characterise the macroscopic organisation of layer crystals in mollusc shells. High degree of order (or texture strength) have been reported [52,26], which vary between taxon with qualitatively identical textures in close species [27], and in a single specimen with the location in the shell, either between different layers [35,53] or in the same layer [24]. As a global scheme, organic macromolecules that form matrices of the shells are controlling the inorganic crystal orientations [22] and also crystal shapes themselves [21], in such a way that these two informations can be seen as non-redundant. Crystal orientations are controlled by intercrystaline organic molecules, while crystal shapes are under the influence of intracrystalline molecules. Crystallographic textures can then provide an information linked to the intercrystalline molecules, i.e. they are the crystalline results of genetic programming. To a certain extend texture is aimed at reflecting genetic influence and can deserve phylogenic interpretations, on a somewhat different aspect compared to SEM investigations. For instance it has been demonstrated that SEM images can misleadingly be interpreted in terms of orientation [27]. QTA has also been proposed to link living species to extinct fossils in the Bivalvia [28].

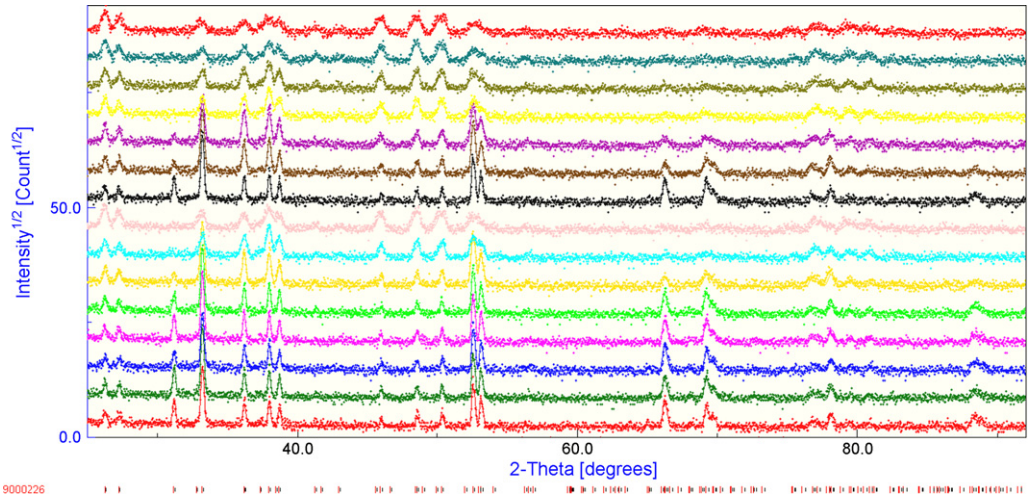

Fig. 2. Randomly selected diagrams with corresponding fits using combined analysis for the inner prismatic layer of *Mercenaria mercenaria*.

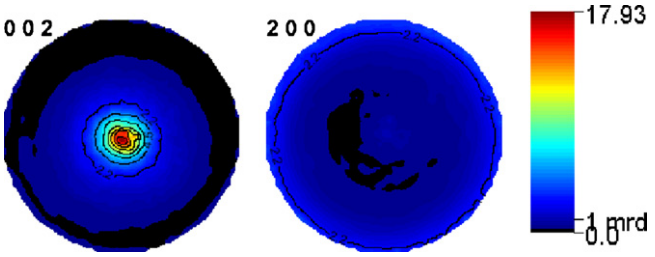

Fig. 3. {002} and {200} normalised pole figures of the inner prismatic layer of *Mercenaria mercenaria*.

4.1. One example of X-ray combined analysis

We illustrate here typical results, taking the example of the inner prismatic layer of *M. mercenaria*. Combined analysis refinements converged in this case to a solution corresponding to good reliability factors, $R_w = 31.53\%$ and $R_{exp} = 26.28\%$, giving a goodness of fit of 1.44. Reliability factors might appear as large compared to literature. However one has to bear in mind that such factors are depending on the number of measured points, which in our case is around 1.8×10^6, with 1900 points/diagram and 936 diagrams. The refinement quality can be visualised by visualising the combined analysis fits on experimental and recalculated diagrams selected at random among the measurements (Fig. 2). The OD reliability factors, $R_w = 12.49\%$ and $R_B = 20.65\%$, compare well with the literature for similar texture strengths [54]. This layer exhibits a moderate texture strength with a texture index of 10.44 m.r.d.^{2} and a maximum OD value of 59.41 m.r.d., as usual for fibre textures observed in clams and phylogenetically closeby species measured up to now. The minimum OD value is 0, as for all other layers studied up to now, indicating that all crystallites are oriented within the texture components. The {002} pole figure shows a broad maximum distribution density in its centre around 18 m.r.d. (Fig. 3) also revealing the moderate strength of the texture, and indicating the tendency of the crystallites to align their *c*-axis along **N**. The {200} pole figure indicates a fibre character with no macroscopic alignment of *a*- and *b*-axes in the (**M**, **G**) shell plane.

4.2. Typical a- and c-axes orientation distributions

From all the layers measured we could observe a variety of crystal orientations that can be summarised using simple symbols for their *c*- and *a*-axes orientations relative to the shell main frame. Dealing with *c*-axis orientations (Fig. 4), the orientation component(s) of either aragonite or calcite can be represented by four different types. If the *c*-axis are normal to the shell surface (with the maximum of the distribution aligned parallel to **N**), we symbolise this texture by ⊥ (Fig. 4a). For *c*-axis inclined with respect to **N** by an angle α, a ∠ symbol is used (Fig. 4b). Some species exhibit dispersions from **N**, which is represented by ∀ (Fig. 4c), or show splitted *c*-axis ∨ (Fig. 4d). Concerning *a*-axis distributions ∀ (Fig. 5), the specimens exhibit single-crystal like characters, as denoted by a | symbol (Fig. 5a), or a fibre texture with *a*-axis at random around *c*-axis (◯, Fig. 5b), or single- or double-twin like patterns (× and * in Fig. 5c and d respectively). In all these figures we give an example for a given layer of a given species, the whole stacking sequence representing the whole shell thickness being represented by as many texture terms.

4.3. Textural nomenclature and terms

A description of the microstructure (crossed lamellar, nacre, sheet nacre), if efficient and widely used in the mollusc literature, cannot unequivoquely and always represent correctly the large range organisation of the crystals with respect to each others. Not only sometimes an SEM image looks homogeneous but exhibits a strong texture [27], but also, for instance regular lamellas can exhibit perfect fibre-like textures [35]. More subtle details of the orientation components can also be inaccessible to SEM, unless EBSD can be operated successfully, like twin characters. This is simply due to the absence of crystal planes probing in imaging techniques using electrons. When electron diffraction can be operated, it remains often a local-to-global scale transfer difficulty, which sometimes prevents easy interpretation.

A compact description of the textural behaviour of layers is useful for an efficient comparison between samples [26]. For a particular layer, L, in the shell, we specify the *c*- and *a*-axes orientations, and quantify the presence and amount of twinning using

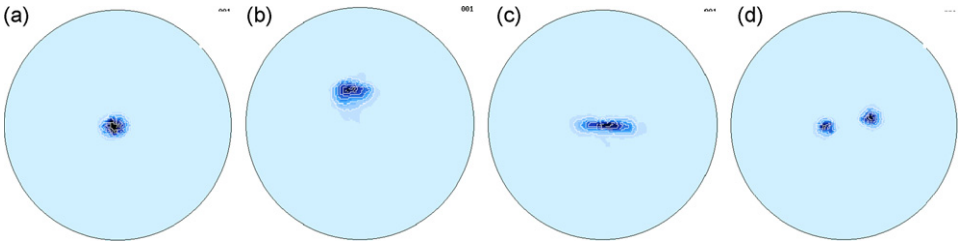

Fig. 4. Typical {001} pole figures representing the various types of orientation for the *c*-axis, e.g. normal orientation ⊥ (*Pinctada maxima*) (a), tilted *c*-axis ∠ (*Nerita polita*) (b), dispersed-axes ∀ (*Fragum fragum*) (c) and split *c*-axis ∨ (*Cypraea testudinaria*)) (d). Equal area projections.

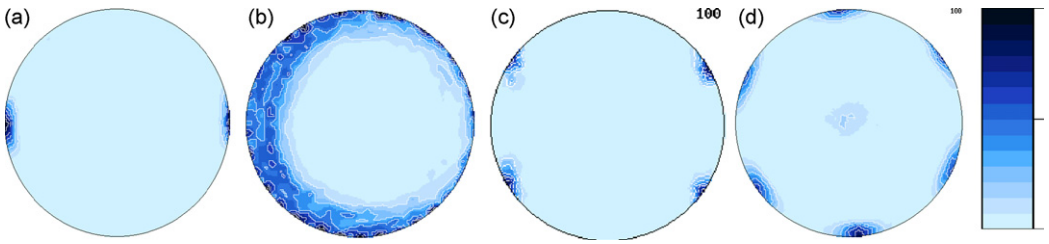

Fig. 5. Typical {100} pole figures representing the various types of orientation for the *a*-axis, e.g. single-crystal like | (*Helix pomatia*) (a), fibre like ◯ (*Tectus niloticus*) (b), single-twin like × (*Conus leopardus*) (c) and double-twin like * (*Nautilus pompilius*) (d). Equal area projection.

the following texture terms. These terms are:

$$\langle c, \alpha | L | P_T^{a,\beta} \rangle \quad (1)$$

where L includes the location of the layer in the shell (inner, outer, intermediate, etc.), its SEM or microscopy microstructural characteristics (comarginal, radial, homogeneous). The left hand side of the bracket describes the *c*-axis pattern (⊥, ∠, etc.). The right hand side describes the *a*-axis pattern (|, *, etc.). Both *a*- and *c*-axes patterns can show a random orientation, which would be schematised by ●. In these terms the angle β represents the angle that makes the lowest-index direction in the sample plane (perpendicular to **N**) with **G**. The T-number is the percentage of twinned volume. We can evaluate the percentage of twinned volume by the {1 0 0} pole density ratio (taken at maximum of the dispersion) of the poles corresponding to the twinning, to all the components. For a single twin activation, we call this volume $T = V_{\times}$, and $T = V_{*}$ for a double twinning. The calculation gives maxima of $V_{*} = 67\%$ for a double twinned pattern and $V_{\times} = 50\%$ for a single twinned layer.

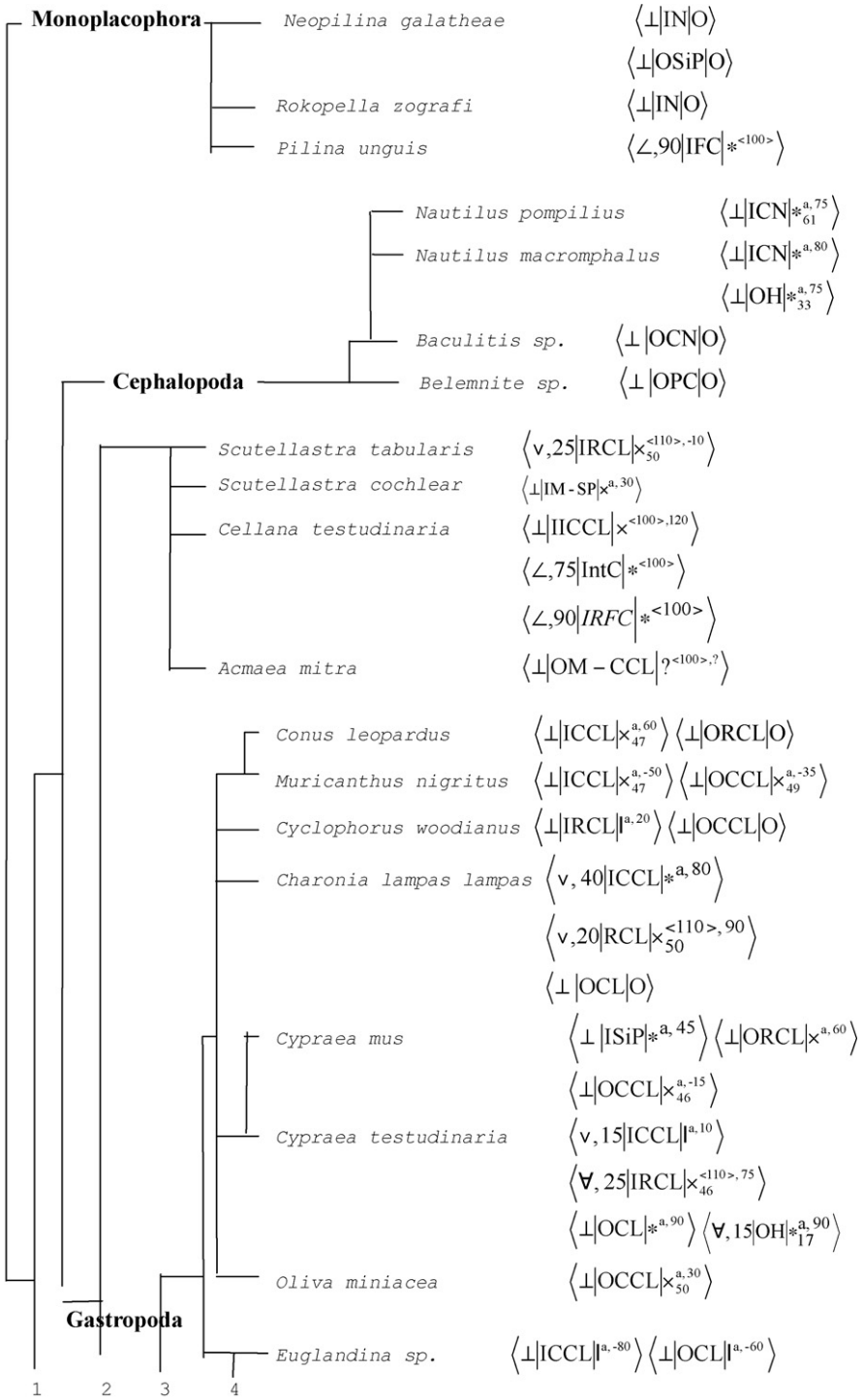

Fig. 6. Proposal for a phylogenetic tree, including textural patterns. The layer acronyms are: I, Inner; Int, intermediate; O, outer; CCL, co-marginal crossed lamellar; RCL, radial crossed lamellar; CoCL, complex crossed lamellar; CoCoCL, cone complex crossed lamellar; CN, columnar nacre; SN, sheet nacre; P, prismatic; H, homogeneous; SiP, simple prismatic; SpP, spherulitic prismatic; ICCL, irregular complex crossed lamellar; IM, inside myostracum; OM, outside myostracum; ICP, intersected crossed platy; OP, operculum; RFC, regularly foliated calcite; HC, homogeneous calcite; PC, prismatic calcite.

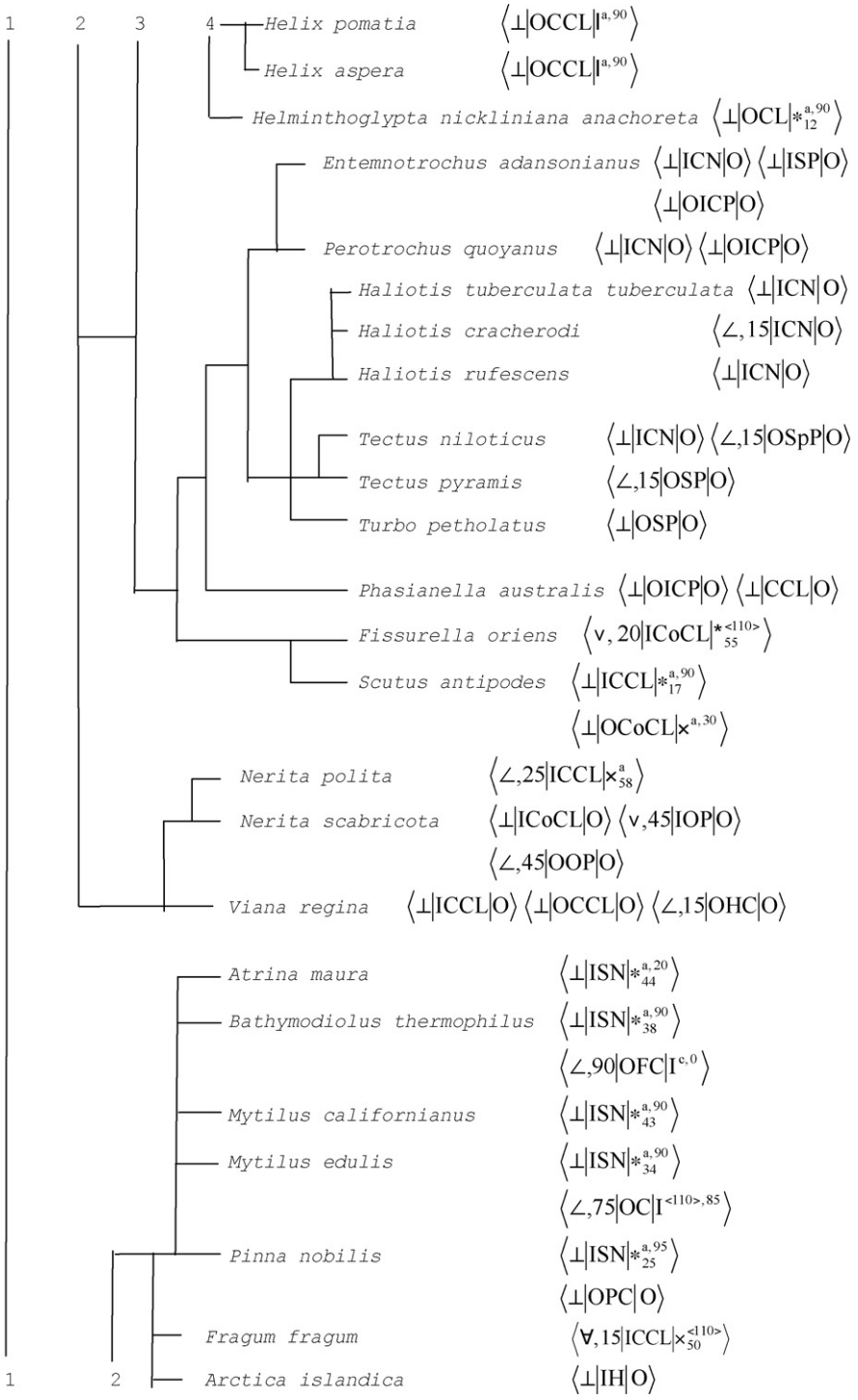

Fig. 6. (*Continued*)

We have not included still in this term the texture strength or entropy, because we still have not detected from our specimen sampling peculiar information from them.

Using these textural-microstructural descriptions (Fig. 6), the shell resemblance and differences can rapidly be checked. For instance *Conus*, *Murycanthus*, *Cyclophorus* and *Charonia* sp. clearly show very close texture terms for their inner and outer layers composed of crossed lamellar microstructures. However, the generally admitted ORCL layer of *Conus leopardus* and OCCL layer of *C. woodianus* both exhibit a fibre texture character. This points out the ambiguity of SEM investigation in such layers, since Radial or Comarginal character cannot be a valid name for a fibre texture with no alignment relationship between cell parameters of different crystallites in the (**G**, **M**) plane. SEM is too much a local probe to be able to ascertain the radial or comarginal character, similarly as what we found in *C. lampas* [35]. We already pointed out the strong similarities of nacre layers for close species, and somewhat different in distant species [26]. This fact is reinforced with the added species of this work, for instance comparing the texture terms of *H. tuberculata*, *A. cygnea*, *M. edulis* or *B. thermophylus* with their respectively closely related taxa. Using the sequence of texture terms which represents the whole shell thickness, for instance to compare

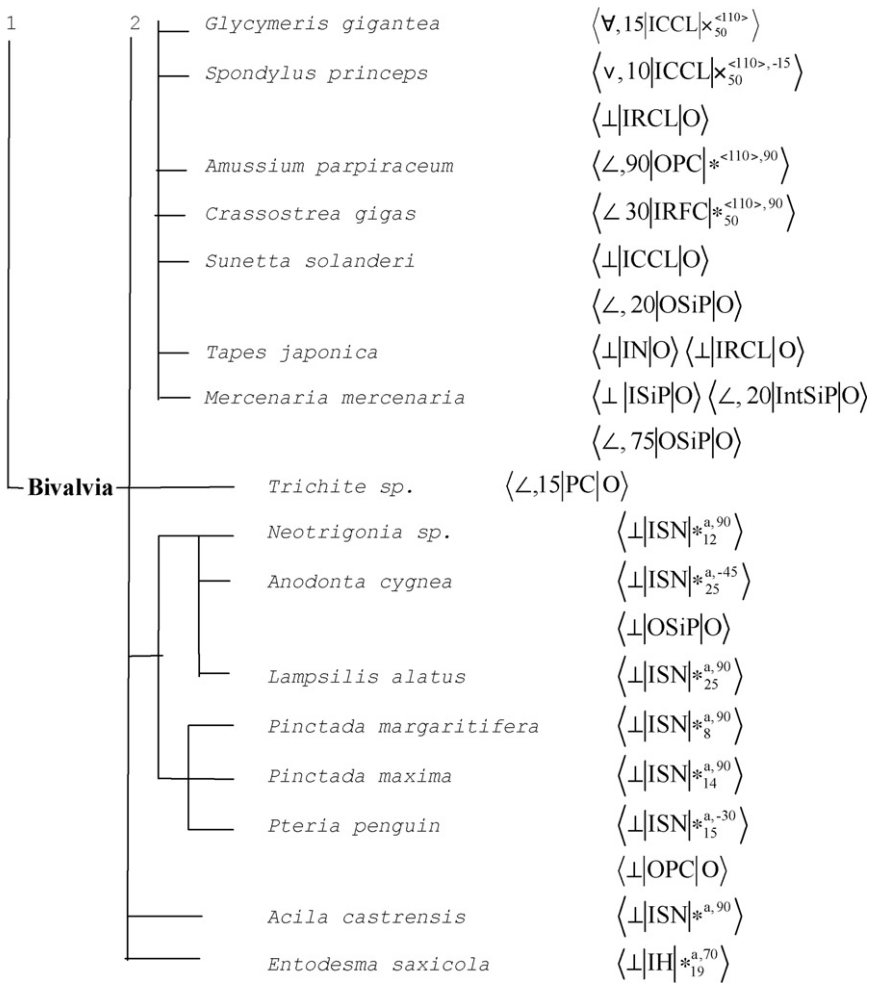

Fig. 6. (*Continued*).

C. testudinaria and *C. lampas*, one can illustrate the quantitatively small differences justifying their phylogenic distance, but also their qualitative similarity pointing for their close relationship. With the newly added species and layers texture terms we could not see more variability of *a*- and *c*-axes texture patterns. In particular, all the calcite layers measured up to now could be represented using the same terminology. Texture variations with thickness from the interior towards the outside of the shell still show outmost layers usually having less orientation degrees than innermost layers, with the prime consequence of fibre textures dominating the shells outsides. Interestingly, the species showing interesting behaviours in terms of medical applications (*P. maxima*, *P. margaritifera*, *P. nobilis*, *H. tuberculata*), also exhibit similar texture terms, and these latter acquiring then a potentially predictive character in this direction.

4.4. Mollusc phylogeny and ancestral nacre

From previous analysis we know there is a non-trivial relationship between the crystallographic textures (orientation distribution of crystals) and shell ultrastructures of mollusc shells [55,53,52,27,35]. Textures differ in shell structures with similar morphological patterns between distantly related molluscs, and may vary between layers within an individual. There is not a one-to-one relationship between shell structures and textures. It becomes legitimate to imagine some phylogenic signal from texture characterisation, since texture is imposed by biological molecules and that we see large variability of texture patterns among the mollusc species investigated to date. It would be premature to operate a full phylogenic analysis covering all the Mollusca from our still limited sampling. At best we can aim to reveal if specific microstructures exhibit enough texture variations among species and use these latter to test their phylogenic impact on some phylogenic hypotheses. Nacre layers appear a good choice for such a test since they show a limited number of patterns, with *c*-axis along **N**, and fibre textures (columnar nacres) or double twinning patterns with various twinned volume amounts (sheet nacres). Twinning also occurs in other microstructural layer types, and can deserve good phylogenic signal. Nacre is also present in the whole Mollusca, and represents the larger sampling of our study. For instance, the inner nacre layer of *N. macromphalus* exhibits double twinning, while the one of *Haliotis* species exhibits fibre textural character. However, we only found single twinning or low V_*'s in gastropods and bivalves, which may signify that the selection of a single twin plane or the growth with small amount of twins is a less ancestral feature in nacre. This would be coherent to the gain in entropy observed, for instance, from *C. mus* or *P. margaritifera* to the *Nautiloidea*.

There are no comprehensive, published phylogenies, applying reproducible techniques to explicit data that analyse the deep roots and also have some resolution in crown groups. To solve this problem, we adopted the molluscan phylogeny proposed by Salvini-Plawen and Steiner [56], incorporated the investigated taxa of this work into the appropriate places, and omitted clades we did not investigate. We present this resulting phylogenetic hypothesis in Fig. 7a. Note that this serves as a basis for our discussion, and is not the result of an analysis. We are not aware of any data capable of producing this particular result. On this tree we indicated in black

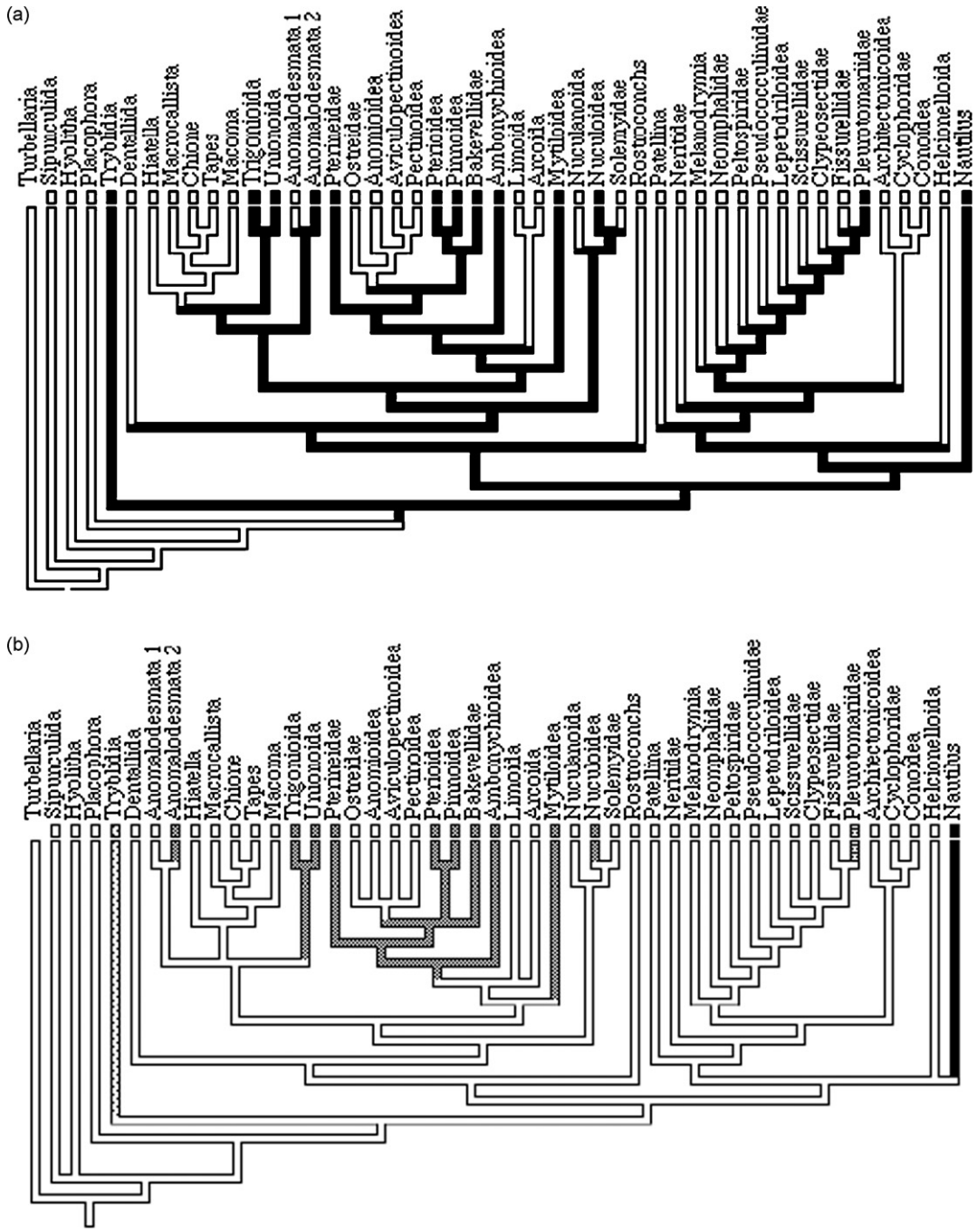

Fig. 7. (a) Phylogenetic tree as proposed by Salvini-Plawen and Steiner [56], limited to the species we studied here (from Tryblydia). Black branches are nacre occurrences. (b) Previous tree after parcimonial analysis, including textural patterns of nacre.

the branches giving rise to species in which nacre is stabilised, the first nacre occurrence starting at the Tryblydia node. The underlying assumption of this tree is that the major clades, gastropods and bivalves in particular, are monophyletic. Its probably so, but strictly speaking it is not tested by any of the quoted analyses. We also have to assume, taxon sampling does not affect the analysis appreciably. That is, we assume substituting *Nerita polita* and *N. scabricota* for "Neritidae" in the analysis of Salvini-Plawen and Steiner [56], will not affect the topology of the gastropod tree. One can see on this hypothesis, and only assuming nacre events, that 20 times nacre is abandoned for another microstructural type. Incorporating the textural characteristics of nacre (Fig. 7b) accomplishes more parsimony in the tree, with only 9 nacre events (8 creations, 1 abandon) and close textural patterns at close phylogenetic distances.

Characterising the texture of more species and layers in the future will give the possibility to test the validity of our analysis. Particularly, one needs to incorporate non-nacre layer textures in the phylogenetic hypothesis, and combine it with calcite layer textures. Our goal here was only to illustrate the use of texture terms as a phylogenetic issue, perhaps to establish in the future a more systematic analysis.

5. Fossil textures and ancestors

We investigated 6 layers from fossilised shells, one from the Monoplacophora (*P. unguis*), 4 Cephalopods (*Baculitis* sp. and 3 *Belemnite* sp. rostra) and one bivalve (*Trichite* sp. from Jurassic). All these layers are made of calcite except *Baculitis* which kept its nacre microstructure.

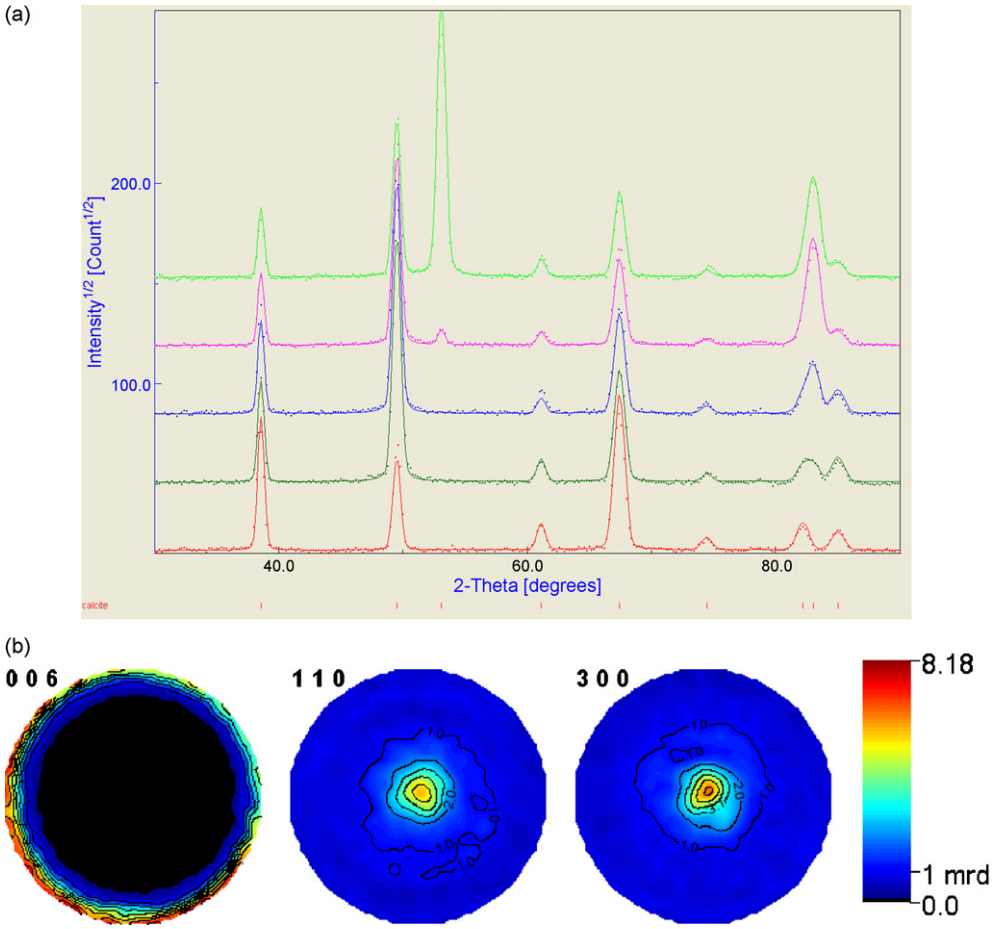

Fig. 8. (a) Randomly selected neutron diffraction diagrams measured at the D1B beamline of ILL on a *Belemnite* rostrum from the *Cretaceous*, and associated combined analysis fits. (b) Corresponding {0 0 6}, {1 1 0} and {3 0 0} pole figures. The centre of the pole figures corresponds to the revolution axis of the rostrum.

Belemnite rostra are composed of calcite prisms having their long axes coinciding with the *c*-axis of the calcite structure, radially arranged around the revolution axis of the rostrum. The prisms are large grains not suitable to the probed scale of X-rays, and we used the D1B and D20 neutron beamlines of the ILL centre (Grenoble, France), to measure the rostra textures. We cut out of the rostrum a slightly conical, 1 cm in height, cylinder at one third of the total length from the rostrum tip. We placed the revolution axis of the cone parallel to the φ axis of the Eulerian craddle. We measured 3 rostra at total, one from the Sarthe bassin, Le Mans, France, and two from the Jurassic and upper Cretaceous. These latter were collected from a relatively oxiding, calcareous, and reducing chalky clays environments respectively. Neutron diffraction diagrams are correctly reproduced from the combined analysis fits (Fig. 8a), and the OD are obtained for instance on the *Cretaceous Belemnite rostrum* with R_w = 13.16% and R_B = 12.50%. The main axes pole figures (Fig. 8b) show that *c*-axis are randomly distributed along the rostrum revolution axis, *a*-axis of calcite being at random around *c*-axis from crystal to crystal. This results in a planar texture, as seen from neutron experiments that probe the whole specimen volume, which corresponds to a fibre texture at a more local scale (as seen from instance using X-rays) with calcite *c*-axis perpendicular to the rostrum at each point of its surface. The corresponding associated texture term is $\langle\perp|\mathrm{OPC}|\mathrm{O}\rangle$ (Fig. 6). We observed the same texture on the two other *Belemnite* rostra, with only slight texture strength variations, and also in the nacre layer of *Baculitis*. In Cephalopods, the two other measured species, *Nautilus*, exhibit double twinning, more ordered nacre layers, with texture entropies much lower than the ones of fibre textures of shells [26]. That is to say, as far as our textural signal can be used, that crystalline organisation at the macroscale of the Cephalopod nacre shells increased with time (lowering texture entropy). Considering that calcite is the most stable polymorph of calcium carbonate under normal conditions, the stabilisation of nacre (aragonite) from Belemnitoids to *Baculitis* then Nautiloids also needs an entropic gain. These two facts also favour more ancestral calcite than aragonite (and consequently nacre) layers.

Our *P. unguis* specimen is the one already studied by Erben et al. [57], whom found its inner shell layer to be composed of thin, continuous layers of calcite blades, which they interpreted as recrystallised nacre. Aragonite is less stable than calcite during diagenesis and consequently finding calcite in the shells of *P. unguis* fossils is not surprising. It is very unusual to find original aragonite in Palaeozoic and Mesozoic fossils, but calcite is common, though it may be either original, recrystallised or replaced calcite. We wish to determine whether the laminar calcite from the inner layer of *P. unguis* is original or indeed recrystallised, by comparing its texture to other SEM-similar mollusc layers. The other laminar-like calcite layers investigated here are from the extant taxa *C testudinaria* and *C. gigas* with inner foliated layers. The texture terms (Fig. 6) of *P. unguis* and the two other taxa ($\langle\angle$, 90|IFC|$*^{\langle 1\,0\,0\rangle}\rangle$, $\langle\angle$, 90|IRFC|$*^{\langle 1\,0\,0\rangle}\rangle$ and $\langle\angle 30|\mathrm{IRFC}|*_{50}^{\langle 1\,1\,0\rangle,90}\rangle$ respectively) strongly point out the pole figures (Fig 9a) resemblance between *P. unguis* and *C. testudinaria*, and residual nacre is totally absent in *P. unguis* (Fig. 9b). In the two former inner layers, the *c*-axis ({0 0 1} pole figures) are aligned close to the growth direction of the shell, at quite 90° from the shell's normal, while in *C. gigas c*-axis are by far closer to the normal of the shell, around 30°. In *P. unguis* the

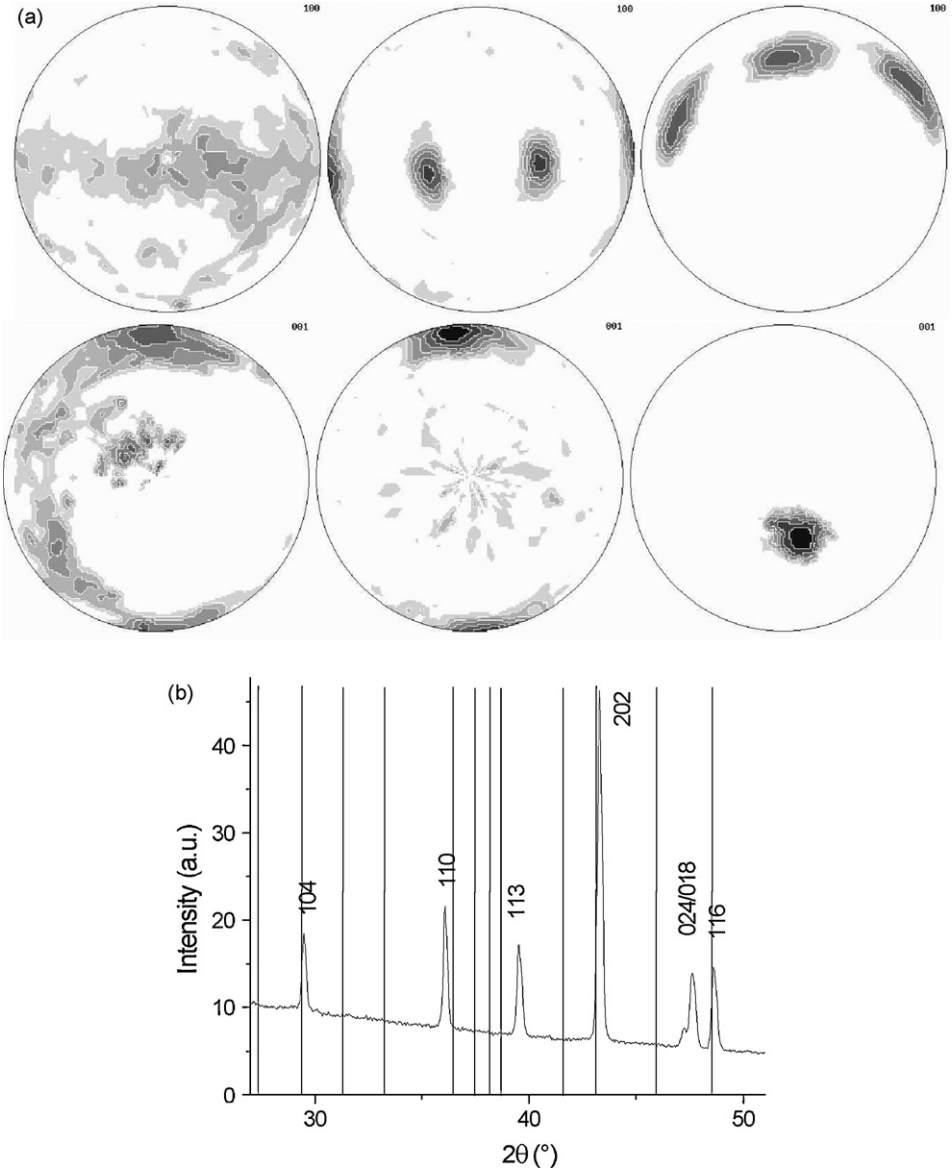

Fig. 9. (a) {0 0 1} (top row) and {1 0 0} (bottom row) recalculated-normalised pole figures of the lamina calcite layers of *Pilina unguis*, *Celana testudinaria* and *Crassostrea gigas*. (b) Powder X-ray diffraction pattern for *Pilina unguis* showing the absence of aragonite (even residual) in the layer.

a-axis distribution is larger than in *C. testudinaria*, but still shows maxima around the same positions, both showing reinforcements along the growth lines direction. Up to now no nacre has been found exhibiting non-normal *c*-axis in mollusc shells. The probably most energetically favourable scheme to recrystallise nacre into calcite would be to transform the pseudo 6-folded axis of symmetry of the former (*c*-axis of aragonite) into the *c*-axis of the hexagonal calcite. This would then have been operated in *P. unguis* with a 90° rotation of all the structure, which looks unlikely to preserve the total shell shape. Erben et al. [57] find the calcite lamellae in *P. unguis* are thicker than nacre tablets of *Nautilus* and *Haliotis* and interpret this as an effect of recrystallisation. Extant Monoplacophora have inner sheet nacre layers, composed of aragonite, and the key question is whether aragonite can recrystallise to calcite, retaining the morphology of the shell structure. Sandberg [58] describes why it is impossible to preserve morphological integrity on a microscopic scale during recrystallisation. The main point is, recrystallisation is mediated by water that needs to be in contact with all recrystallising molecules, i.e. the material needs some porosity, and a certain volume of material must be removed. Aragonite has the specific gravity 2.93 and calcite 2.71 – there are approximately 8% more molecules in a given volume of aragonite than in calcite – and during recrystallisation volume has to expand or material be removed, which is impossible without disrupting morphology. Erben et al. [57] ascribe thickening of lamellae to recrystallisation, which is not plausible. Recrystallisation is a three-dimensional process, and it is not possible to retain two dimensions, expanding the third only. Furthermore, Bøggild [59] always describe recrystallised shells as "irregularly grained calcite", composed of coarse calcite grains without common crystallographic orientation. Our previous works have come to let us expect very strong textures from extant aragonite mollusc shell structures, and the texture patterns from calcite layers indicate calcite shell structures have similarly strong textures. The texture pattern of *P. unguis* is weaker than those of *C. testudinaria* and *C. gigas*, and the specimen may contain diagenetic calcite as well as shell material, that might have been exposed to minor recrystallisation, disturbing textures, or weak textures may be characteristic of early Monoplacophora. The inner shell layer of the fossil *P. unguis* shares the properties – morphology, dimensions and texture (orientation distribution) – of calcite deposited by

similar processes in a sister taxon. It is most parsimonious to interpret the shell structures of *P. unguis* as original, largely unaltered, and thereby as regularly foliated [33], than as recrystallised nacre. Regular foliated shell structure has the same mineralogy and morphology as the laminar calcite observed by Erben et al. [57] and ourselves. The dimensions of the observed shell structure correspond better to regular foliated, and this interpretation does not necessitate the assumption of novel physical processes. Modern Monoplacophora unquestionably have nacreous shells [60,57,61], but *P. unguis* does not. It seems that Mesozoic or Palaeozoic monoplacophoran described in the literature does not too. The HAM (Hypothetical Ancestral Mollusc), largely modelled on *N. galatheae*, has all but vanished from modern literature, yet it is still virtually an axiom of molluscan evolution that a nacreous shell is plesiomorphic (e.g. [62–64,56]). It is beyond our scope to evaluate that classic assumption, but believe we have presented evidence against the only tangible observation that could support that assumption.

Traditionally, *Trichites* is placed within the Pinnoidea, a pteriomorph group, which normally have regular ham-shaped shells and live partially embedded in soft sediments, anchored by abyssal threads. Pinnoids do have flexible shells comprised of thin layers of calcite prisms, lined internally by nacre. *Trichites* appears to adopt a rather different life habit, lying on one side on top of the sediment and is frequently highly distorted and display torsion, therefore implying that if it is indeed a pinnoid it is a rather aberrant form. Further examination of the crystallographic textures of *Trichites* and comparison of those from recent pinnoids and pteriomorphians may provide a better means of determining their relationships. There are some hypotheses to suggest that the earliest bivalves were all entirely aragonitic and of rather simple construction from two microstructural types. However, later bivalves evolved a further 5 microstructural types (2 of them calcitic) and utilised these in a variety of different arrangements. The result is that the bivalve microstructure and mineralogy is extremely diverse across the class and is, therefore, thought to be a valuable character for phylogenetic analysis. Two major types of calcite microstructure are identified: prisms, which usually occur on the outside of the valve, and foliated which tends to occupy the bulk of a shell (e.g. oysters: *C. gigas*). Of these calcite prisms are perhaps the most interesting because there is good evidence that calcitic prisms have evolved at least four times independently within the Bivalvia, in the mussels, pterioids, chamids and the extinct rudists. Looking at prismatic calcite layers of the sub-class Pteriomorphia, we encompass two of the calcite secreting clades, the mussels and the pterioids. It is therefore, of great value to compare the orientation of the calcite crystals within members of these taxa. *Bathymodiolus thermophilus* and *M. edulis* are both mussels, the former being an important component of deep sea vent faunas. Although both have calcitic outer shell layers it is clear from texture analysis (Fig. 6) that the two are separate innovations of the calcitic shell layer, with different alignment schemes of their *a*-axis, compared to *P. nobilis*, *P. penguin*, *Trichites* sp. and *A. parpiraceum*. Although these ostensibly all belong to the same clade of calcite secretors it is important to establish the degree of similarity or difference between these various taxa. In particular, recent molecular schemes have placed the pteriids (i.e. *P. penguin*) as a sister-group to the pinnoids (*Pinna* and possibly *Trichites*). All three species exhibit similar textures, but *Trichites*, if we except its slightly inclined *c*-axis distribution, shows an ODF maximum closer to the pinnoids than to the pteriids [28]. *A. parpiraceum* belongs to the superfamily Pectinoidea which, according to some phylogenetic schemes at least, is further removed from the pteriids and pinnoids, than are the mussels. If this is so, then calcite secretion in the pterioid group may be polyphyletic and thus we might expect the *Amussium* to display different textures to the Pinna + Pteria and the mussels. This is actually what we have measured as textures in *Amussium*, which presents a clearly not random alignment of its *a*-axis (i.e. is different of *Trichites*, Pteriids and Pinnoids), a *c*-axis distribution in the plane of the shell and <1 1 0> directions aligned with **M** (where *B. thermophilus* has its *a*-axis). The taxonomic position of *Trichites*, from the texture terms point of view (of the calcite layer), would root Pinnoids and Pterioids, though of course one would have to test more species, and in particular some aragonite layers of *Trichites*.

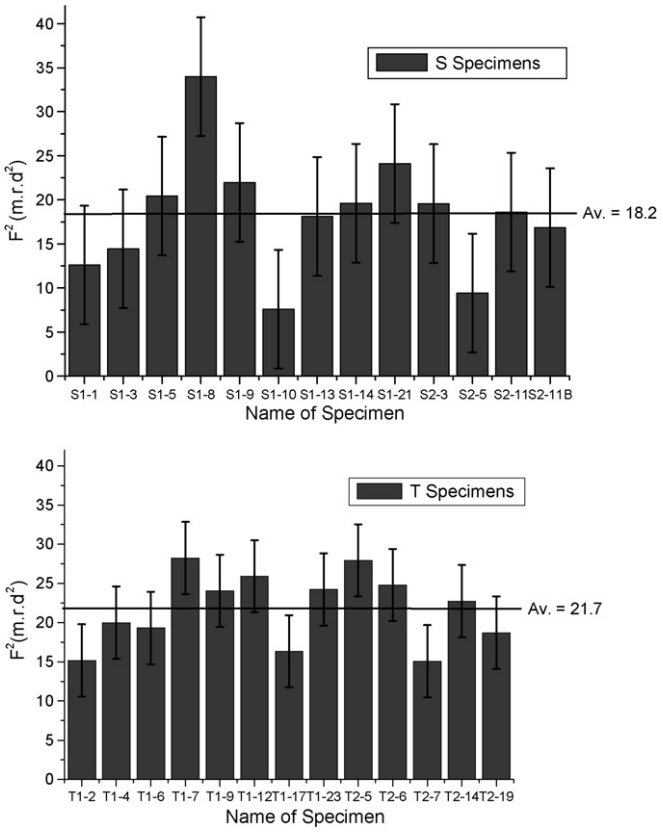

Fig. 10. (a) F^2 Histogram for S specimens with an average of 18.2 m.r.d.^{2}, including an error bar indicating the standard deviation for the entire set: 6.7 r.m.s. and (b) F^2 histogram for C specimens with an average of 21.7 m.r.d.^{2} including an error bar indicating the standard deviation for the entire class: 4.5 r.m.s.

6. Texture variability on a given species, and farming

One could raise the question on how much a texture signal can vary within repeated measurements, or for a given species. We decided to test this reliability on *H. aspersa aspersa* shells (Section 2). Selected snails used here are issued from the 7th generation of selection. Their mean weight is 16.98 g against 10.61 g for the control snails. Fourteen and fifteen samples are analysed in this work, for the C and S lines respectively. They were chosen in the whole population available with weight and age close to the population means. Shell specimens were all prepared the same day according to the following way: animals were frozen at −18 °C and thaw after 1 day. On 29 measured individuals, the texture refinement reliability factors ranged from approx. 12% to 32% (with 5–6 r.m.s. standard deviation on the average values), with a slight tendency to larger ODF max and texture strengths in the control samples, even if both sets overlap within their standard deviations [36]. On these two parameters (ODF max and F^2) standard deviations on average values are lower for C samples than for S, as can be seen for instance on histograms (Fig. 10)with standard deviations. The significantly stronger textures observed for C's underlines the achievement of a higher degree of orientation in control samples. Smaller standard deviation of F^2 in C compared to S indicates a larger textural resem-

Table 1
Combined analysis results for the layers on which combined analysis could characterise structural distortions. Parentheses are standard deviations on the last digit. GoF: goodness of fit. Cell parameters and atomic positions references for the non-biogenic aragonite are from Caspi et al. [41].

Shell	*Charonia lampas lampas*			*Pinctada maxima*	*Haliotis tuberculata tuberculata*	*Mercenaria mercenaria*		
Layer	OCL	IRCL	ICCL	ISN	ICN	OSiP	IntSiP	ISiP
a (Å)	4.98563(7)	4.97538(4)	4.9813(1)	4.97071(4)	4.9480(2)	4.9455(3)	4.95311(8)	4.95713(6)
b (Å)	8.0103(1)	7.98848(8)	7.9679(1)	7.96629(6)	7.9427(6)	7.93863(6)	7.9453(1)	7.95315(9)
c (Å)	5.74626(3)	5.74961(2)	5.76261(5)	5.74804(2)	5.7443(6)	5.72453(5)	5.73292(2)	5.73329(2)
$\Delta a/a$	0.0048	0.0027	0.0039	0.0018	−0.0028	−0.0033	−0.0018	−0.0009
$\Delta b/b$	0.0052	0.0024	0.0002	−0.0004	−0.0033	−0.0038	−0.0030	−0.0020
$\Delta c/c$	0.0006	0.0012	0.0034	0.0009	0.0003	−0.0032	−0.0017	−0.0017
Ca								
y	0.41418(5)	0.414071(4)	0.41276(9)	0.41479(3)	0.41418(5)	0.41282(4)	0.41431(5)	0.41462(5)
z	0.75939(3)	0.76057(2)	0.75818(8)	0.75939(2)	0.75939(3)	0.75814(7)	0.75904(4)	0.75723(5)
C								
y	0.7628(2)	0.76341(2)	0.7356(4)	0.7676(1)	0.7628(2)	0.7413(2)	0.7589(4)	0.7506(3)
z	−0.0920(1)	−0.08702(9)	−0.0833(2)	−0.0831(1)	−0.0920(1)	−0.0814(2)	−0.0802(2)	−0.0851(2)
O1								
y	0.9115(2)	0.9238(1)	0.8957(3)	0.9134(1)	0.9115(2)	0.9197(2)	0.923(3)	0.9302(2)
z	−0.09205(8)	−0.09456(6)	−0.1018(2)	−0.09255(7)	−0.09205(8)	−0.1008(1)	−0.0963(1)	−0.0972(1)
O2								
x	0.4768(1)	0.4754(1)	0.4864(3)	0.4678(1)	0.4768(1)	0.4837(2)	0.4735(2)	0.4717(2)
y	0.6826(1)	0.68332(9)	0.6834(2)	0.68176(7)	0.6826(1)	0.68746(8)	0.6818(1)	0.6918(1)
z	−0.08368(6)	−0.08473(5)	−0.0926(1)	−0.09060(4)	−0.08368(6)	−0.087(1)	−0.08925(9)	−0.08999(9)
ΔZ_{C-O1} (Å)	0.00029	0.04335	0.1066	0.054	0.00029	0.111	0.092	0.069

blance in between the standard specimens than in the ones selected for increased weight. The overlap of the results (including standard deviations) tells us that the overall preferred crystallite orientation is only mildly dependent on the selection carried out, though the degree of this orientation is slightly influenced. The texture terms are not modified by selection, but ODF (or F^2) values, indicating that the direction of the preferred orientation of the crystallites does not change with selection, but the number of crystallites that orientates does. The shells investigated here are far from flat which is a strong factor toward variability of results using X-ray investigations. We carefully took specimens having the same size, and studied a piece of shell always at the same distance from the margin. The texture strength variability detected in this work illustrates the quantitative parameters variability but the constant texture terms. Quantitative variability will depend on the specimen surface, but can be approached with the study of many samples, as operated here.

7. Structural distortions in biogenic crystals

It has been demonstrated by Pokroy et al. [8–10] that aragonite unit-cells are distorted in mollusc biocrystals, and that atomic positions (structures) are also modified compared to inorganic references. Unit-cell distortions are anisotropic, and structural distortions reflect the aplanarity of the carbonate group of aragonite. The choice of the aragonite reference is crucial in such a study, and we took a geological aragonite for which very precise structural determination was operated [41]. Up to now only 4 species could be analysed using combined analysis to give access to these distortions on a real sample (non-powderised layers), on several layers eventually (Table 1). The refined cell parameters of all the layers exhibit cell distortions compared to non-biogenic aragonite. However, only the nacre and prismatic layers show some cell parameter contraction, in the (**a**, **b**) plane of aragonite. The cell distortions are anisotropic and the relative volume variations variable among the layers of different shells as well as in the same shell. We measured real layers, not powderised nor bleached, and the distortions observed come from both intercrystalline and intracrystalline molecules. Even with intercrystalline molecules associated to the calcium carbonate polymorph selection, and to the peculiar crystallites organisation in the shells, one cannot exclude an effect of these former on the cells distortion. Since it exists strong bonding between these molecules and the mineral to promote orientation, they also are probably largely responsible for the anisotropic character of the unit-cell distortion. This would explain why our cell distortions are larger than the ones observed in the case of solely intracrystalline molecules remain [9]. All the textured layers show unit-cell distortion anisotropy, and the most deformed cell parameters depend on the layer type. There is then a strong relationship between the way the unit-cells are deformed and the layer texture. For instance, all cell parameters are extended in the measured crossed lamellar layers, while the nacre and prismatic layers exhibit compressed (**a**, **b**) planes and a rather constant or elongated *c*-axis. One should notice that no residual stress could be detected in the layers. All molecules are then intimate parts of new biocomposite crystals and not only intercalated entities deserving new stabilised states of known crystals. In the case of *C. lampas*, second order lamellaes are inclined with respect to the *c*-axis of aragonite [35]. This gives rise to a global expansion of the unit-cells, while in nacres in which substructures of each nacre platelet is parallel to their plane, the cell distortions appear more anisotropic. The cell distortion is clearly different between the two observed nacres. In the columnar nacre the (**a**, **b**) planes appear compressed along the two main directions, though slightly, while for sheet nacre a small compression is only observed along **b**, and an elongation along **a**, both remaining much smaller in magnitude than in the ICN layer of *H. tuberculata*. This anisotropy of the distortion in the (**a**, **b**) plane for ISN layers could be another illustration of the observation of Mutvei and Dunca [65] when submitting ISN to preferential etching by sodium hypochlorite, while absent in ICN of *H. tuberculata*. The case of prismatic layers of *M. mercenaria* is particularly interesting, since all the cell parameters are compressed, slightly, which includes compression in the (**a**, **b**) plane as in nacres. This deformation similarity of hexagonal-like shaped bio-crystallites could be the result of similar intracrystalline molecules in both nacres and prismatic layers, if proved in the future on more species layers.

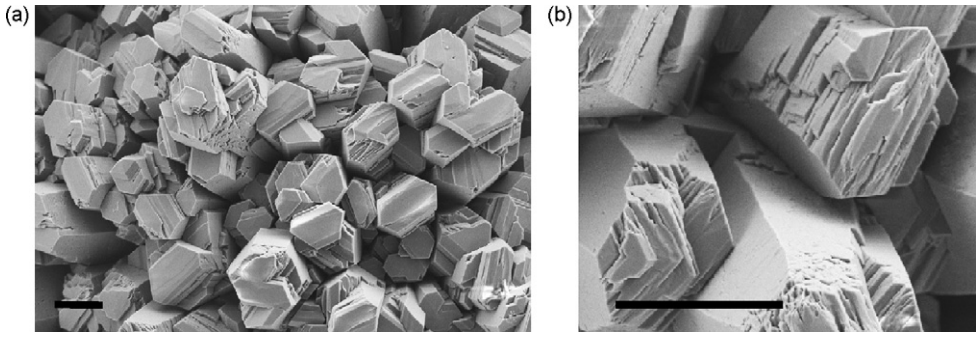

Fig. 11. (a) Hexagon-like prisms of pure aragonite as obtained using electrodeposition on titanium foils and (b) zoom on the previous crystals showing 60° orientation relationships in the prisms, and their tendency to delamination into hexagon slabs. Scale bars are 1 μm.

The refined atomic positions were obtained without refinement of thermal vibrations, because of the lack of sensitivity on these latter in our diffraction range. The distance $\Delta Z_{C-O1} = (z_C - z_{O1})c$ between carbon and oxygen planes reveals aplanarity of the carbonate groups [9]. This distance goes from 0 for calcite, to 0.057 Å for non-biogenic aragonite reference. We already discussed the atomic position variations in the crossed lamellar layers of *Charonia* [66], which could express, together with the loss in texture strength, the progressive control loss of organic matter farther from the animal. In the two analysed nacre layers, the ΔZ_{C-O1} values are intermediate compared to the ones of *Charonia*, but there is a clear tendency for a larger one in the columnar layer of *Haliotis*, which

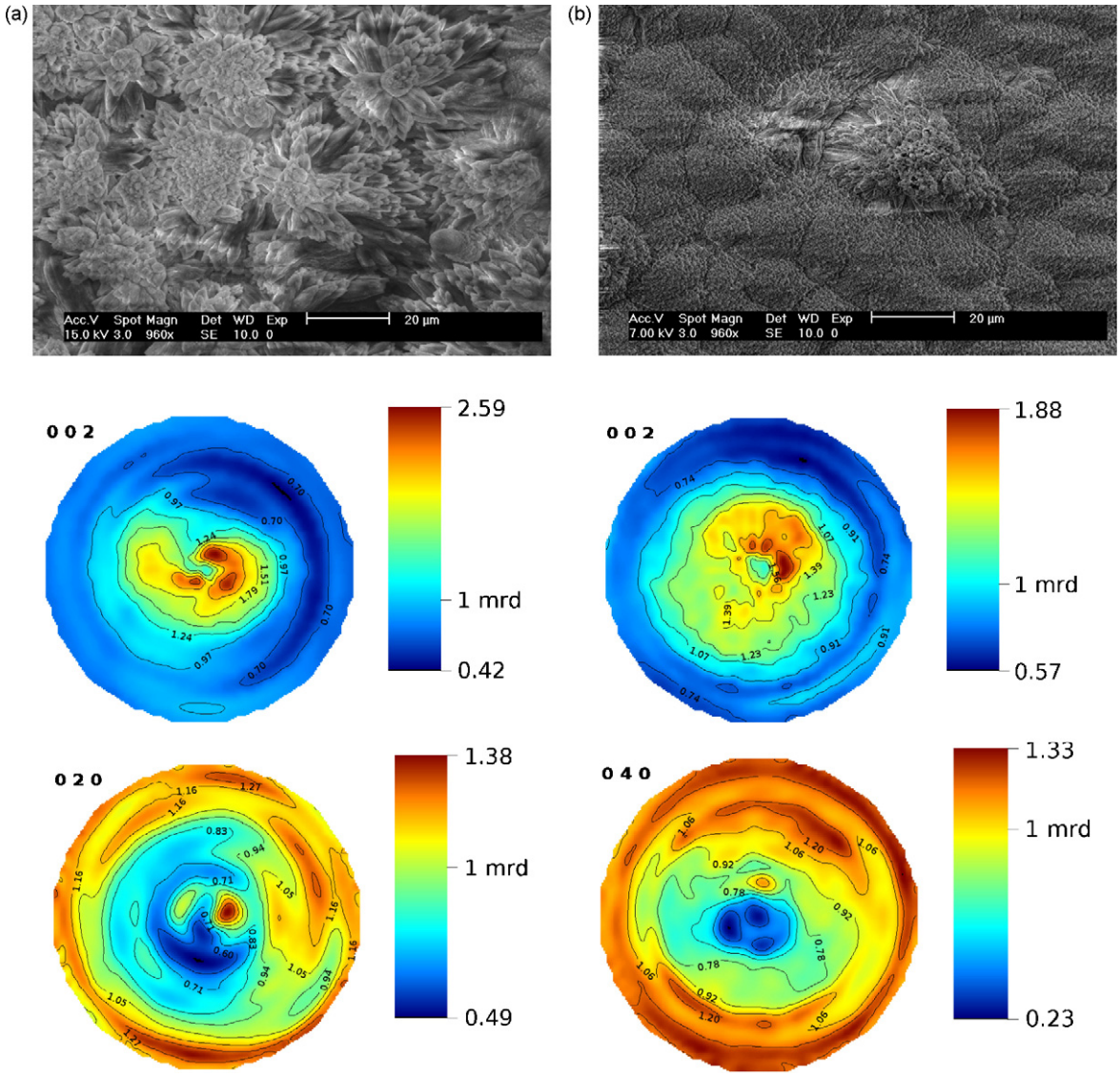

Fig. 12. SEM images and {0 0 2} and {0 4 0} pole figures of aragonite films on Ti foils, with addition of organic extrata during electrodeposition: (a) addition of WSM and (b) addition of ESM.

Table 2
Combined analysis results for the electrodeposited aragonite layers on titanium foils.

Organic addition	None	Chitosan	WSM	ES
$\Delta a/a$	0.0011	−0.0004	0.0019	−0.0008
$\Delta b/b$	0.0017	0.0000	0.0015	−0.0009
$\Delta c/c$	0.0007	0.0000	0.0017	0.0001
ΔZ_{C-O1} (Å)	0.087	0.040	0.135	0.173

would correspond to a larger stabilised energetic state if the crystals were entirely inorganic with such an aplanarity. The ΔZ_{C-O1} values for the prismatic layers of *M. mercenaria* are as large as for the ICCL layer of *C. lampas*. The carbonate groups aplanarity is on average larger in this species than in all others studied up to now.

8. Nacre coatings on Ti substrates

In a previous work [17] we demonstrated the possibility to deposit hexagon-like prismatic layers on medical-grade titanium foils, using electrodeposition. This work paves the way to deposition of aragonitic layers on all kinds of real prostheses, since electrochemistry a priori does not show strong limitations on the shape to be covered. Such fully inorganic layers (Fig. 10a) were moderately textured, with {0 0 1} pole figure maxima around 5 m.r.d., but with fibre textures and perpendicular *c*-axis represented by $\langle \perp|CaCO_3/Ti|O \rangle$ texture terms, similar to many nacre layers of species from many classes. Furthermore, the prisms of our layers exhibit a neat tendency to intrinsic delaminating (Fig. 11b), looking like premises of hexagonal slabs, though not fully segmented. This tendency can be viewed to a first sight as a way to accommodate metastable energy of aragonite. The individual platelets outlined this way look alternatively at 60° on top of each others along the prism column, as illustrated on natural columnar nacres by Mutvei and Dunca [65]. We probably synthesised aragonite layers very close to the microstructure of gastropod columnar nacres, if texture strength is out of concerns. The atomic positions in such aragonite films correspond to ΔZ_{C-O1} values of prismatic layers, but with unit-cell distortions as small as the ones of sheet nacres.

Another interesting feature of electrodeposition relies in the possibility to incorporate organics in the electrolyte, at least in weak volumic amounts, as for natural biocrystallisation. We incorporated into the electrolyte organics either as chitosan or as extracted from *P. margaritifera*, these latter being either the water-soluble (WSM) or the ethanol-soluble (ESM) matrix fractions of the shell [38]. Unit cell distortions and atomic positions modifications (Table 2) are not identical for all the additions. Chitosan addition practically does not modify unit-cells or atomic positions, and is probably not entering the crystal structure. WSM gives rise to a unit-cell expansion on the three cell parameters with slight anisotropy of the deformation, while ESM operates slight compressions of the (**a**, **b**) planes and very small expansion along **c**, similarly as what is observed in the natural columnar nacre of *H. tuberculata*. Both extract produce the largest carbonate group aplanarity observed up to now. Interestingly, SEM images of these films (Fig. 12) show irregular six-edged polygons, in particular in the case of ESM addition. Furthermore pole figures show a weak but significant orientation keeping the same texture term as for inorganic aragonite films. While WSM addition tends to maintain a relatively large texture (with 2.6 m.r.d. at the maximum of the {0 0 2} pole figure) but to disorganise significantly the crystal hexagonal aspects, ESM operates reversely. These organic–inorganic hybrid films show that different extract, and in particular their polar (WSM) or non-polar (ESM) character, have different effects on crystallisation and orientation of aragonite crystals. WSM would then act more as intercrystalline molecules do in natural nacres, while ESM would play the intracrystalline role.

9. Conclusion

Mollusc phylogeny for the bivalves, gastropods, cephalopods and monoplacophoran clades has been regarded from the texture pattern point of view. Compared to our previous works, more species and layers have been added to the experiments, together with fossils and calcitic layers. We extended also the analysis not only to texture patterns, but to structural modifications. These latter are proved to vary between species and layers and could appear in the future as providing more character analysis. The texture terms applied on mollusc nacres can be used to propose a more parcimonious classification than usually agreed with ancestral nacre, at least on the base of the still restricted number of analysed species. Also the texture terms can be used to provide some characters for the link between extinct and extant species, via the analysis of calcitic and aragonite layers of some fossils. We showed that using electrodeposition, organic–inorganic composite layers can be deposited on medical grade titanium substrates, which show structural distortions close to the ones encountered in some natural species. Reliability of texture analysis has been measured in a statistical approach on *H. aspersa*, and show good reproducibility.

Acknowledgments

The authors are grateful to B. Ouladdiaf, ILL Grenoble, France, M. Dupont-Nivet, INRA Jouy-en-Josas France, Elisabeth Harper, Dept. Earth Sciences Cambridge UK, H.-R. Wenk, Dept. Earth Planetary Sciences Berkeley, CA USA, Eddy Poty, Univ. of Liège Belgium.

We would like to thank the following institutions and individuals for making specimens available for this study:

The University of California Museum of Paleontology, Berkeley USA, The Naturhistoriska Riksmuseet in Stockholm kindly gave us access to the *Pilina unguis* specimens, The United State National Museum of Natural History, USA, The Zoologisk Museum, Copenhagen Denmark, The MARVEL (1997) expedition (Responsible: Daniel Desbruyeres, Laboratoire d'écologie abyssale, département environnement profond, IFREMER Brest for the *Bathymodiolus thermophilus* specimen, Françoise Denis, Laboratoire de Biologie et Génétique Evolutive, Université du Maine, Le Mans-France for the *Anodonta cygnea* specimen, Barry Roth kindly helped with the identification of *Helminthoglypta nickliniana anachoreta* and of *Euglandina* sp., The French Ministère de l'Education Nationale, de la Recherche et des Technologies, for providing one of us (D.C.) with a one-year post-doctoral fundind at University of California at Berkeley, The French Région Basse-Normandie for its partial funding of the X-ray texture instrument, Institut Laue-Langevin, Grenoble France for neutron scattering experiments).

References

[1] M.A. Cariolou, D. Morse, Journal of Comparative Physiology B 157 (6) (1988) 717–729.
[2] P.E. Hare, P.H. Abelson, Year Book, vol. 65, Carnegie Inst., Washington, 1965, pp. 223–232.
[3] J.D. Currey, Proceedings of the Royal Society of London B: Biological Sciences 196 (1125) (1977) 443–463.
[4] A.P. Jackson, J.F.V. Vincent, R.M. Turner, Journal of Materials Science 25 (7) (1990) 3173–3178.
[5] S. Kamat, X. Su, R. Ballarini, A.H. Heuer, Nature 405 (6790) (2000) 1036–1040.
[6] B.L. Smith, T.E. Schaffer, M. Viani, J.B. Thompson, N.A. Frederick, J. Kindt, A. Belcher, G.D. Stucky, D.E. Morse, P.K. Hansma, Nature 399 (6738) (1999) 761–763.
[7] B. Chen, X. Peng, J. Wang, S. Sun, Computational Materials Science 44 (2008) 201–205.
[8] B. Pokroy, J.P. Quintana, E.N. Caspi, A. Berner, E. Zolotoyabko, Nature Materials 3 (12) (2004) 900–902.
[9] B. Pokroy, A.N. Fitch, P.L. Lee, J.P. Quintana, E.N. Caspi, E. Zolotoyabko, Journal of Structural Biology 153 (1) (2006) 96–103.

[10] B. Pokroy, J.S. Fieramosca, R.B. Von Dreele, A.N. Fitch, E.N. Caspi, E. Zolotoyabko, Chemistry of Materials 19 (13) (2007) 3244–3251.
[11] A. Bobbio, Bulletin of the Historical Dentology 20 (1972) 1–6.
[12] G. Atlan, O. Delattre, S. Berland, A. LeFaou, G. Nabias, D. Cot, E. Lopez, Biomaterials 20 (1999) 1017–1022.
[13] E. Lopez, B. Vidal, S. Berland, S. Camprasse, G. Camprasse, C. Silve, Tissue and Cell 24 (5) (1992) 667–679.
[14] G. Atlan, N. Balmain, S. Berland, B. Vidal, E. Lopez, Comptes Rendus de l'Académie des Sciences Série III: Sciences de la Vie 320 (3) (1997) 253–258.
[15] E. Lopez, A. Le Faou, S. Borzeix, S. Berland, Tissue and Cell 32 (1) (2000) 95–101.
[16] M. Rousseau, L. Bedouet, E. Lati, P. Gasser, K. Le Ny, E. Lopez, Comparative Biochemistry and Physiology B: Biochemistry & Molecular Biology 145 (1) (2006) 1–9.
[17] C. Krauss, D. Chateigner, O. Gil, Crystal Growth and Design 8 (12) (2008) 4378–4382.
[18] S. Weiner, W. Traub, Philosophical Transactions of the Royal Society of London Series B 304 (1984) 425–434.
[19] A. Berman, L. Addadi, A. Kvick, L. Leiserowitz, M. Nelson, S. Weiner, Science 250 (1990) 664–667.
[20] J.G. Carter, Skeletal Biomineralisation: Patterns, Processes and Evolutionary Trends, Van Nostrand Reinhold, New York, 1990.
[21] J. Aizenberg, M. Ilan, S. Weiner, L. Addadi, Connective Tissue Research 34 (4) (1996) 255–261.
[22] G. Falini, S. Albeck, S. Weiner, L. Addadi, Science 271 (1996) 67–69.
[23] M.J. Almeida, C. Milet, J. Peduzzi, L. Pereira, J. Haigle, M. Barthelemy, E. Lopez, Journal of Experimental Zoology 288 (4) (2000) 327–334.
[24] A. Checa, A. Rodriguez-Navarro, Biomaterials 26 (2005) 1071–1079.
[25] M. Rousseau, E. Lopez, P. Stempfle, M. Brendle, L. Franke, A. Guette, R. Naslain, X. Bourrat, Biomaterials 26 (2005) 6254.
[26] D. Chateigner, C. Hedegaard, H.-R. Wenk, in: J.A. Szpunar (Ed.), Textures of Materials, vol. 2, NRC Research Press, Ottawa, 1999, pp. 1495–1500.
[27] D. Chateigner, C. Hedegaard, H.-R. Wenk, Journal of Structural Geology 22 (2000) 1723–1735.
[28] D. Chateigner, M. Morales, E.M. Harper, Materials Science Forum 408–412 (2002) 1687–1692.
[29] D. Duplat, M. Puissegur, L. Bedouet, A. Rousseau, H. Boulzaguet, C. Milet, D. Sellos, A. Van Wormhoudt, E. Lopez, FEBS Letters 580 (10) (2006) 2435–2441.
[30] C. Hedegaard, Shell structures of the recent Archaeogastropoda, PhD Thesis, University of Aarhus, Denmark, vol. 1 & 2, 1990.
[31] J.D. Taylor, W.J. Kennedy, A. Hall, Zoology 22 (9) (1973) 253–294.
[32] J.G. Carter, in: D.C. Rhoads, R.A. Lutz (Eds.), Skeletal Growth of Aquatic Organisms, Plenum, New York, 1980.
[33] J.G. Carter, G.R. Clark II, in: D.J. Bottjer, C.S. Hickman, P.D. Ward, T.W. Broadhead (Eds.), Molluscs Notes for a Short Course, University of Tenessee Department of Geological Sciences Studies in Geology, 1985, pp. 50–71.
[34] C. Hedegaard, Journal of Molluscan Studies 63 (1997) 369–377.
[35] S. Ouhenia, D. Chateigner, M.A. Belkhir, E. Guilmeau, Journal of Structural Biology 163 (2008) 175–184.
[36] D. Chateigner, R. Kaptein, M. Dupont-Nivet, American Malacological Bulletin 27 (1–2) (2009) 157–165.
[37] M. Dupont-Nivet, J. Mallard, J.-C. Bonnet, J.-M. Blanc, The Journal of Experimental Zoology 287 (2000) 80–85.
[38] M. Rousseau, L. Pereira-Mouries, M.J. Almeida, C. Milet, E. Lopez, Comparative Biochemistry and Physiology B: Biochemistry & Molecular Biology 135 (1) (2003) 1–7.
[39] C. Krauss, Couches polycristallines orientées d'aragonite biomimétique, synthétisées par voie électrochimique, PhD Thesis, Université de Caen Basse-Normandie, 2009, 172 pp.
[40] S. Gražulis, D. Chateigner, R.T. Downs, A.F.T. Yokochi, M. Quirós, L. Lutterotti, E. Manakova, J. Butkus, P. Moeck, A. Le Bail, Journal of Applied Crystallography 42 (4) (2009) 726–729, http://www.crystallography.net/.
[41] E.N. Caspi, B. Pokroy, P.L. Lee, J.P. Quintana, E. Zolotoyabko, Acta Crystallographica B 61 (2005) 129–132.
[42] D. Chateigner (Ed.), Combined Analysis, ISTE - John Wiley & Sons, 2010, p. 496, ISBN-10: 1-84821-198-8, ISBN-13: 978-1-84821-198-8, http://www.wiley-vch.de/publish/en/books/ISBN978-1-84821-198-8.
[43] M. Morales, D. Chateigner, L. Lutterotti, J. Ricote, Materials Science Forum 408–412 (2002) 113–118.
[44] M. Morales, Y. Leconte, R. Rizk, D. Chateigner, Journal of Applied Physics 97 (2005) 034307-1–134307-13.
[45] J. Ricote, D. Chateigner, G. Ripault, L. Pardo, M. Alguero, J. Mendiola, M.L. Calzada, in: J.A. Szpunar (Ed.), Textures of Materials, vol. 2, NRC Research Press, Ottawa, 1999, pp. 1327–1332.
[46] L. Ratschbacher, B.R. Hacker, L.E. Webb, A. Calvert, T.R. Ireland, M.O. McWilliams, S. Dong, D. Chateigner, H.-R. Wenk, Journal of Geophysical Research 105 (B6) (2000) 13303–13338.
[47] S. Miro, D. Grebille, D. Chateigner, D. Pelloquin, J.-P. Stoquert, J.-J. Grob, J.-M. Costantini, F. Studer, Nuclear Instruments and Methods in Physics Research B 227 (2005) 306–318.
[48] D. Chateigner, P. Germi, M. Pernet, Materials Science Forum 157–162 (1994) 1379–1386.
[49] H.-R. Wenk, S. Matthies, J. Donovan, D. Chateigner, Journal of Applied Crystallography 31 (1998) 262–269.
[50] L. Lutterotti, S. Matthies, H.-R. Wenk, National Research Council of Canada, Ottawa, 1999, pp. 1599–1604. http://www.ing.unitn.it/~luttero/maud.
[51] H.-R. Wenk, Journal of Applied Crystallography 24 (1991) 920–927.
[52] C. Hedegaard, H.-R. Wenk, Journal of Molluscan Studies 64 (1998) 133–136.
[53] D. Chateigner, C. Hedegaard, H.-R. Wenk, in: Z. Liang, L. Zuo, Y. Chu (Eds.), Textures of Materials, vol. 2, 1996, pp. 1221–1226.
[54] D. Chateigner, Journal of Applied Crystallography 38 (2005) 603–611.
[55] N.V. Wilmot, D.J. Barber, J.D. Taylor, A.L. Graham, Philosophical Transactions of the Royal Society of London Series B 337 (1992) 21–35.
[56] L.v. Salvini-Plawen, G. Steiner, in: J.D. Taylor (Ed.), Origin and Evolutionary Radiation of the Mollusca, Oxford University Press, London, 1996, pp. 29–51.
[57] H.K. Erben, G. Flajs, A. Siehl, Akademie der Wissenschaften un der Literatur, Abhandlungen der Mathematisch-Naturwissenschaftlichen Klasse, Mainz, 1968, pp. 1–24, pl. 1–17.
[58] P.A. Sandberg, Palaeontographica Americana 54 (1984) 272–281.
[59] O.B. Bøggild, Det Kongelige Danske Videnskabernes Selskabs Skrifter, Naturvidenskabelige og Mathematiske Afdeling, vol. 9, Række, 1930, II.2: pp. 231–325, pl. I–XV.
[60] W.J. Schmidt, Galatha Report 3 (1959) 73–77.
[61] M. Taviani, B. Sabelli, F. Candini, Lethaia 23 (1990) 213–216.
[62] K.G. Wingstrand, Scientific Results of The Danish Deep-sea Expedition Round the World 1950–52, vol. 16, 1985, pp. 7–94, pl. 1–12.
[63] G. Haszprunar, American Malacological Bulletin 10 (2) (1993) 165–177.
[64] B. Runnegar, in: J. Taylor (Ed.), Origin and Evolutionary Radiation of the Mollusca, Oxford University Press, London, 1996, pp. 77–87.
[65] H. Mutvei, E. Dunca, Palaeontologische Zeitschrift 82 (1) (2008) 85–94.
[66] D. Chateigner, S. Ouhenia, C. Krauss, M. Belkhir, M. Morales, Nuclear Instruments and Methods in Physics Research B 268 (3–4) (2010) 341–345.